ACS NANO

www.acsnano.org

ARTICLE

Cephalopod-Inspired Chromotropic Ionic Skin with Rapid Visual Sensing Capabilities to Multiple Stimuli

Yunpeng Wang, Xianfei Cao, Jie Cheng, Bowen Yao, Yusen Zhao, Suli Wu, Benzhi Ju, Shufen Zhang, Ximin He,* and Wenbin Niu*

Cite This: *ACS Nano* 2021, 15, 3509–3521

Read Online

ACCESS | Metrics & More | Article Recommendations | Supporting Information

ABSTRACT: **Biological skin systems can perceive various external stimuli through ion transduction. Especially, the skin of some advanced organisms such as cephalopods can further promptly change body color by manipulating photonic nanostructures. However, the current skin-inspired soft iontronics lack the rapid full-color switching ability to respond to multiple stimuli including tension, pressure, and temperature. Here, an intelligent chromotropic iontronics with these fascinating functions is developed by constructing a biomimetic ultrastructure with anisotropic electrostatic repulsion. This skin-like chromotropic iontronics can synchronously realize electrical response and optical visualization to mechanical strain and tactile sensation by adjusting the ultrastructure in cooperation with ionic mechanotransduction. Notably, it can perform instantaneous geometric changes to thermal stimuli *via* an anisotropic electrostatic repulsion interior. Such a capability allows bionic skin to transduce temperature or infrared light into ionic signals and color changes in real time. The design of anisotropic photonic nanostructures expands the intelligent application for soft iontronics at higher levels, providing a concise, multifunctional, interactive sensing platform that dynamically displays stimuli information on its body.**

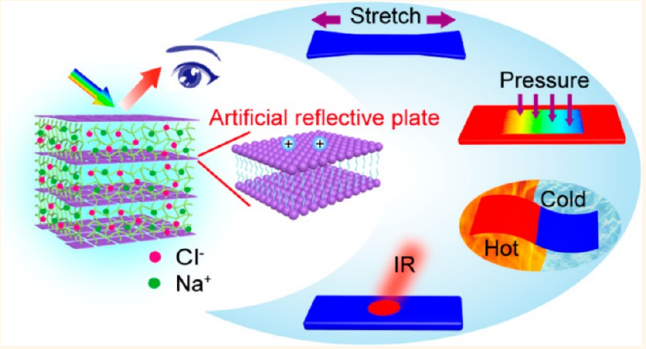

KEYWORDS: *chromotropic iontronics, biomimetic skin, dynamic display, ultrastructures, multifunctional sensing*

Biological skin transforms environmental information into bioelectrical signals and transmits it to the nervous system through ion transport across membranes (Figure 1a), thus perceiving external strain, tactile sensation, vibration, temperature, *etc.*[1−6] Inspired by the ionic transduction of biological skin, soft iontronics is developed for artificial skin and flexible sensory systems as a successor of flexible electronics, owing to its excellent biocompatibility, the same ion language as biological systems, and realistic simulation of biological functions.[5,7−10] Besides bioelectrical signal response, in particular, the skin of some animals (such as tropical fishes,[11] cephalopods,[12,13] and reptiles[14,15]) can further actively perceive the complex environment through color change for communication, courtship, camouflage, and even thermoregulation.[16,17] For instance, cephalopod skin has reflective plates periodically arranged inside iridophores to form photonic nanostructures (Figure 1b) that are well known as one-dimensional photonic crystals (1D PCs).[18−23] This ultrastructure interacts physically with incident light to produce visualized structural colors.[13,23,24] The cephalopods can actively change color within several seconds to minutes by regulating the refractive index and thickness (*i.e.*, lattice spacing) of the reflector. Simulating the color-switching mechanism would impart the iontronics with dual-signal response behavior, in which the ion signal offers precise sensing capability and the color change provides visual information, thus allowing for higher-level applications including multifunctional sensing, visualized dynamic displays, and direct intelligent interactions with users.[25] Therefore, it is of great significance to develop skin-like chromotropic iontronics.

Received: January 7, 2021
Accepted: January 29, 2021
Published: February 2, 2021

https://dx.doi.org/10.1021/acsnano.1c00181
ACS Nano 2021, 15, 3509–3521

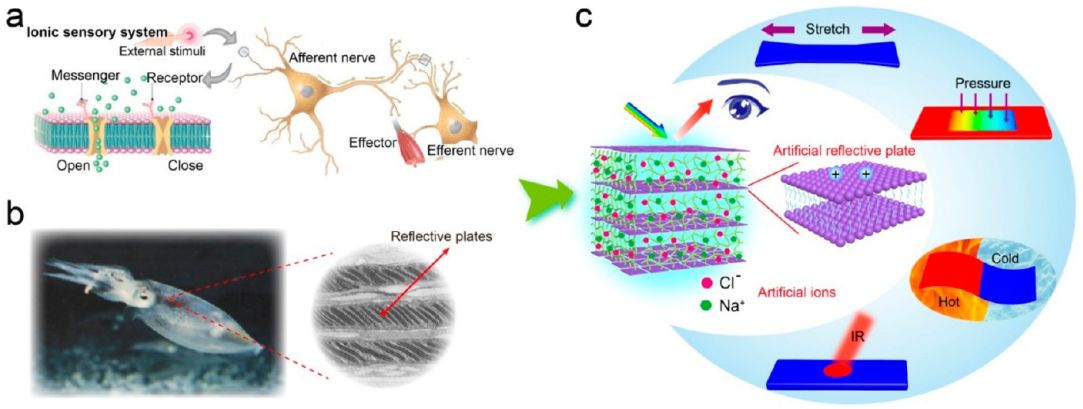

Figure 1. Illustration of a cephalopod-mimicking CIskin. (a) Schematic diagram of a biological ionic sensory system based on ion transport. Adapted with permission from ref 5. Copyright 2020 Wiley-VCH. (b) Image of a rapidly color-changing cephalopod with photonic nanostructures. Adapted with permission from ref 23. Copyright 1990 Springer-Verlag. (c) Illustration of a biomimetic skin with multifunctional visual sensing.

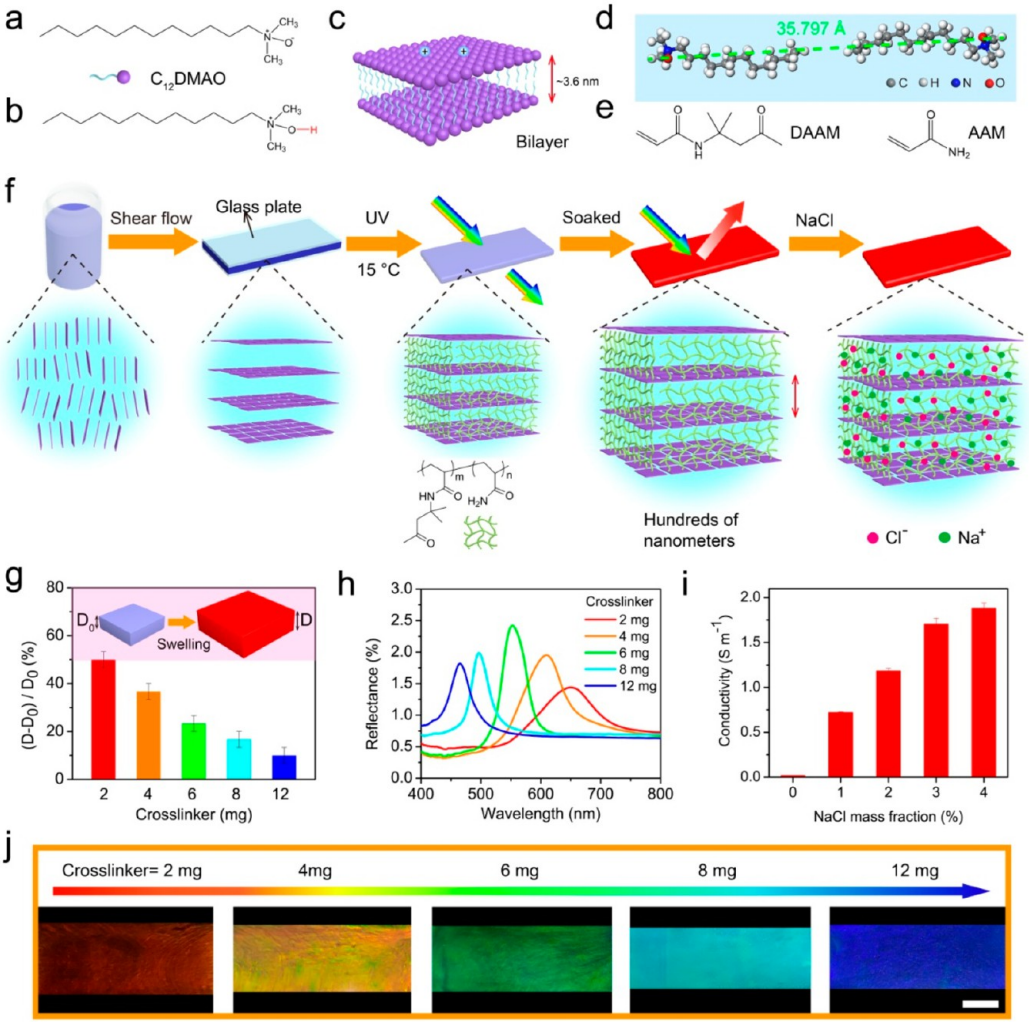

Figure 2. Preparation of ICPH. (a, b) Structural formula of the original (a) and protonated (b) C_{12}DMAO molecule. (c, d) Schematic diagram (c) and thickness (d) simulated by Materials Studio of the C_{12}DMAO bilayer. (e) Polymerizable monomers DAAM and AAM used for forming the hydrogel. (f) Schematic illustration showing the preparation process of ICPH. (g, h) Swelling ratio (g) and the corresponding reflection spectra (h) of hydrogels prepared with different cross-linker contents. (i) Ionic conductivity of hydrogels after soaking in NaCl solutions with different concentrations. (j) Photographs of ICPH with different structural colors at 20 °C. Scale bar is 1 cm.

By integrating electronically conductive carbon or silver nanomaterials with chromotropic elements (*e.g.*, electrochromic dyes, thermochromic dyes, mechanochromic dyes),[26−30] interactive electronic devices that can be switched

https://dx.doi.org/10.1021/acsnano.1c00181
ACS Nano 2021, 15, 3509−3521

between two color states have been developed for strain and tactile sensing. However, it is difficult for them to continuously visualize the intermediate motion states. To address this challenge, we and other researchers employed flexible PCs as optical elements to realize full-color switching in the visible region.[31−33] Despite great advances, the carriers in those devices are electrons and holes, which are difficult to seamlessly communicate with biology due to fundamental difference in information transduction principles of natural skin.[3,4,34] Meanwhile, easy aggregation of conductive materials, uncertain biotoxicity, and undesirable electrochemical reactions with the tissue interface further limit their application in visualized human−machine interfaces.[6,9,35] Therefore, it is highly desirable to develop chromotropic ionic skin (CIskin) that fully mimics the ion transduction and the photonic nanostructures of organisms for tension and pressure sensing and synergistic visualization reporting on its body.

PCs based on a hydrogel matrix (photonic hydrogel), combined with electrolyte salts, provide the potential to serve as ideal candidates for CIskin. The intrinsic stretchability of hydrogels allows them to change color in response to mechanical forces by varying the lattice spacing.[36] At the same time, their interconnected microporous network structure and high water content offer an excellent environment for ion transport. Unfortunately, the preparation of PCs with ionic conductivity characteristics and their application in skin-like iontronics are rarely reported. On the other hand, it is very meaningful to realize multiple visual sensations besides mechanical stimuli. For instance, temperature sensing is a vital function that enables organisms to avoid tissue damage caused by supercooling or overheating. However, it remains a huge challenge because traditional temperature-sensitive PCs exhibit slow color-changing behavior, which is difficult to match the electrical signal response speed of ionic skin.[37−39] Hence, it is imperative to design a class of ultrafast thermochromic photonic hydrogels to visualize the temperature in real time. In addtion, biomimetic skins should be able to perceive light as an extension of perception, especially infrared light (IR), which cannot be observed with the naked eye. Due to radiative heat transfer, organisms are easily burned when exposed to strong IR light; thus, the color sensing of IR light would provide an early visual warning and greatly avoid the above risk. As far as we know, demonstration of a rapidly color-switching biomimetic CIskin that can interactively sense tension, pressure, temperature, and IR light has not been achieved.

In this paper, mimicking the ultrastructures of cephalopod skins, we report a facile but robust design strategy to develop a multifunctional sensing CIskin with optical and ionic dual-signal output synchronously (Figure 1c). The key is to construct a photonic nanostructure with anisotropic electrostatic repulsion inside a thermal-induced permittivity-switchable hydrogel using surface-charged 2D nanomaterials. First, protonated surfactant molecules are self-assembled into positively charged 2D bilayer lamellar structures to simulate the reflective plates in iridophores. Then, they are periodically embedded into a cross-linked hydrogel matrix to form the anisotropic liquid crystal photonic hydrogels to produce reflection color.[36,40,41] Meanwhile, ions (*e.g.*, Na^+, Cl^-) are introduced between the 2D bilayers to emulate the bioelectrical signaling species of skin. Finally, an artificial ionic sensory system based on the above-mentioned ionic-conductive photonic hydrogels (ICPHs) is constructed as biomimetic CIskin. This reasonable material design ensures that tension or stress can change its ion conductivity and lattice spacing synchronously, thus generating electrical and color changes. More importantly, there is an anisotropic electrostatic repulsion inside the unusual photonic nanostructure. By altering the repulsion force through the thermal-induced permittivity switching, the geometry of the ICPH can produce timely anisotropic deformation, realizing ultrafast color switching from red to blue (~0.1 s) and visually monitoring invisible temperature stimuli in real time. In addition, with the virtue of this advantage, our biomimetic skin further demonstrates dual-signal response capability to IR light through a photothermal effect.

RESULTS AND DISCUSSION

Preparation of Ionic-Conductive Photonic Hydrogels.

The reflective plates of ICPHs are constructed using *N*,*N*-dimethyl-1-dodecylamine *N*-oxide (C_{12}DMAO) as a building element. C_{12}DMAO is an amphoteric surfactant (Figure 2a), which can self-assemble into 2D bilayer plate structures and subsequently form lamellar liquid crystals in water, in the presence of a small amount of cosurfactant *n*-hexanol.[42] Owing to protonation of the aminoxide group by water, the C_{12}DMAO bilayers are positively charged (zeta potential, ~6.2 mV, Figure 2b,c). The distance between these bilayers reaches hundreds of nanometers under electrostatic repulsion, thus giving rise to bright structural color *via* Bragg diffraction (Figure S1a). The thickness of the bilayer is approximately 3.6 nm estimated by Materials Studio software (Figure 2d).[43] The transmission electron microscope (TEM) image shows that the bilayer can be up to micron size (Figure S1b). Typically, polymerizable monomers (diacetone acrylamide, DAAM; acrylamide, AAM; cross-linker *N*, *N*-methylene diacrylamide, MBAA) were introduced into a C_{12}DMAO solution, which was slowly injected into a reaction cell composed of two parallel glass plates (Figure 2e,f, Figure S2, Tables S1 and S2). The bilayers were arranged parallel to the glass plates under shear force.[41,44,45] Then, these bilayers were fixed in a poly(diacetone acrylamide-*co*-acrylamide) (PDAAM-*co*-PAAM) network by UV curing; C_{12}DMAO photonic hydrogels were obtained after soaking in deionized water. The small-angle X-ray scattering (SAXS) spectrum does not show a series of typical sharp scattering peaks at the scattering vector (q) ratio of 1:2:3 (Figure S3), indicating that the bilayers are on the order of short-range rather than long-range in the network.[46,47] Finally, we successfully prepared ICPH by introducing ions between bilayers through immersing in a NaCl solution.

Here, we controlled the swelling degree of the hydrogels by adjusting the cross-linker MBAA concentration (Table S2 and Figure S4) and obtained a series of hydrogels with different structural colors from red to blue. The reflection wavelength λ is given by the following Bragg equation:

$$\lambda = 2nd \sin\theta \quad (1)$$

in which n, d, and θ represent the effective refractive index, the lattice spacing, and the incidence angle,[31,41] respectively. Therefore, with the increase of cross-linker, the expansion degree (swelling ratio) of hydrogels along the thickness direction decreased gradually, resulting in a decrease of bilayer spacing d and thus a decrease in reflection wavelength λ (Figure 2g,h and Figure S5). The introduction of Na^+ and Cl^- ions improves the conductivity of ICPH significantly, as shown in Figure 2i. As the concentration of NaCl solution increased (from 1 wt % to 4 wt %), the conductivity was enhanced

https://dx.doi.org/10.1021/acsnano.1c00181
ACS Nano 2021, 15, 3509−3521

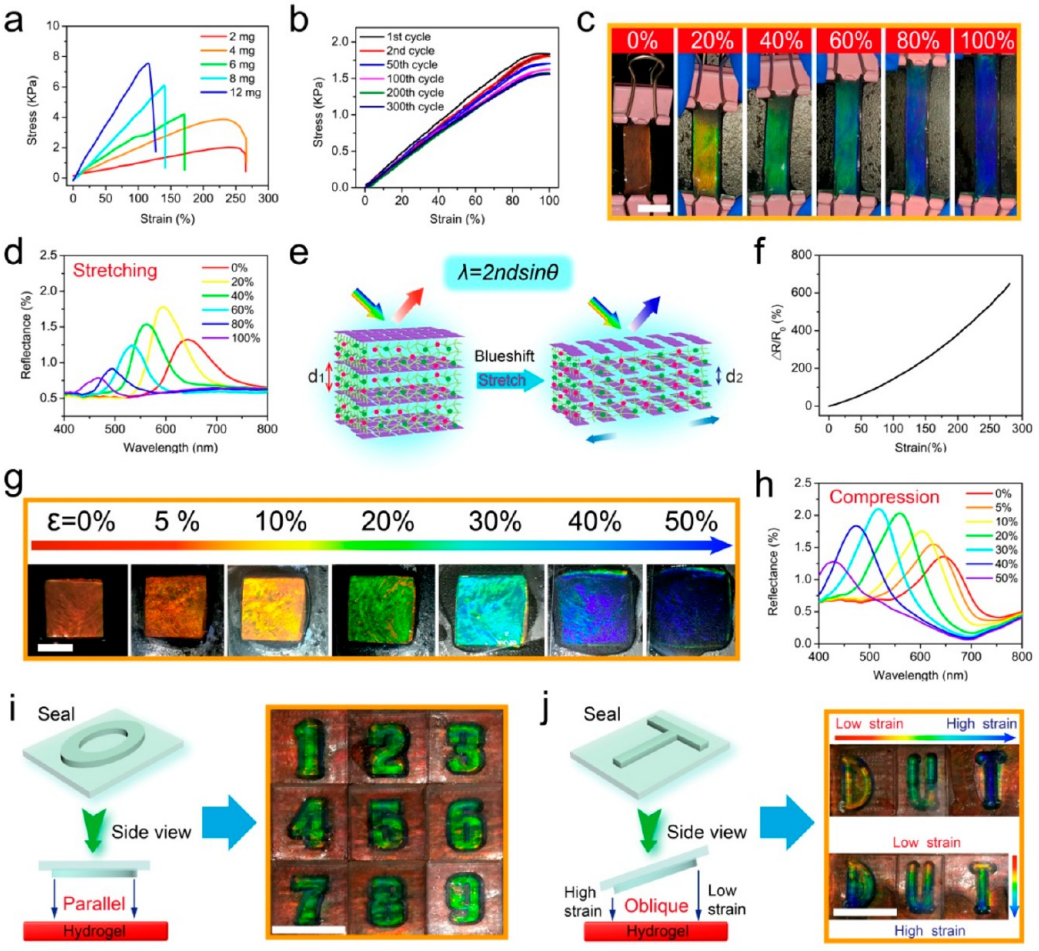

Figure 3. Mechanical, optical, and electrical properties of the ICPH. (a) Stress−strain curves of ICPH prepared with different cross-linker contents. (b) Continuous loading−unloading curve of ICPH at 100% uniaxial tensile strain. (c−f) Photographs of color-switching behavior (c), tensile strain-dependent reflection spectra (d), mechanism illustration (e), and relative resistance change (f) of a red ICPH during stretching. Scale bar in (c) is 1 cm. (g, h) Compressive strain-dependent photographs (g) and reflection spectra (h) of a red ICPH during compressing. Scale bar in (g) is 1 cm. (i, j) Schematic diagram and photographs showing the color changes induced by the convex letters superimposed with a uniform (i) and a gradient stress field (j). Scale bars are 1 cm.

gradually (from 0.72 s m^{-1} to 1.88 s m^{-1}). However, an overly high concentration of NaCl solution causes dehydration and volume shrinkage of the hydrogel matrix because of high osmotic pressure (Figure S6). Considering the relatively high ionic conductivity and stable structural color, the ICPH prepared in 2 wt % NaCl solutions was used as a sensing element for subsequent tests. Correspondingly, a series of ICPHs with bright structural colors are demonstrated, as intuitively shown in Figure 2j.

Optical and Electrical Properties of ICPH under Strain and Pressure. For biomimetic skins, high tensile properties are essential to accommodate arbitrary bending and curved surfaces and to avoid the mechanical damage under large deformation. Figure 3a shows stress−strain curves of a series of ICPHs. Since the hydrogel network gets denser with increasing cross-linking density, the tensile fracture strain decreases, while the fracture stress enhances gradually.[31,48] Typically, the red ICPH has a relatively good tensile strain of ∼250%. Continuous loading−unloading cycles demonstrate its excellent elasticity characteristic (Figure 3b). After a slight hysteresis loop in the first cycle (from 0% to 100%), there is almost no hysteresis in the subsequent cycle curves, suggesting that the hydrogel can quickly recover to its initial state after each stretching.[7,47,49] The stretchability and excellent elasticity of hydrogels are conducive to the dynamic reversible mechanochromism in a large working range, thus realizing the visualization of deformation and interaction with users.

To verify the dynamic color switching from red to blue, we investigated the mechanochromic performance of the red ICPH under tensile and compressive deformations. When the uniaxial tensile strain increases from 0% to 100%, the reflection wavelength λ of the red ICPH shifts continuously from 643 to 465 nm, as intuitively displayed in Figure 3c,d. During stretching, the thickness along the observation direction that is perpendicular to the tensile plane shrinks. Therefore, the λ blue-shifts with decreasing of d according to Bragg eq 1,[31] as shown in Figure 3e. At the same time, the relative resistance ($\Delta R/R_0 = (R - R_0)/R_0$, where R_0 is the initial resistance and R is the test resistance) increases gradually because of the increase in the ion transport distance and decrease in the cross-section area[34] (Figure 3f). Moreover, an analogous blue-shift phenomenon was also presented when the ICPH was compressed, as displayed in Figure 3g,h and Figure S7. Movie S1 records the dynamic change in structural colors during cyclic compression. It is noteworthy that green digital "1−9" patterns appear clearly when a sample was pressed with

https://dx.doi.org/10.1021/acsnano.1c00181
ACS Nano 2021, 15, 3509−3521

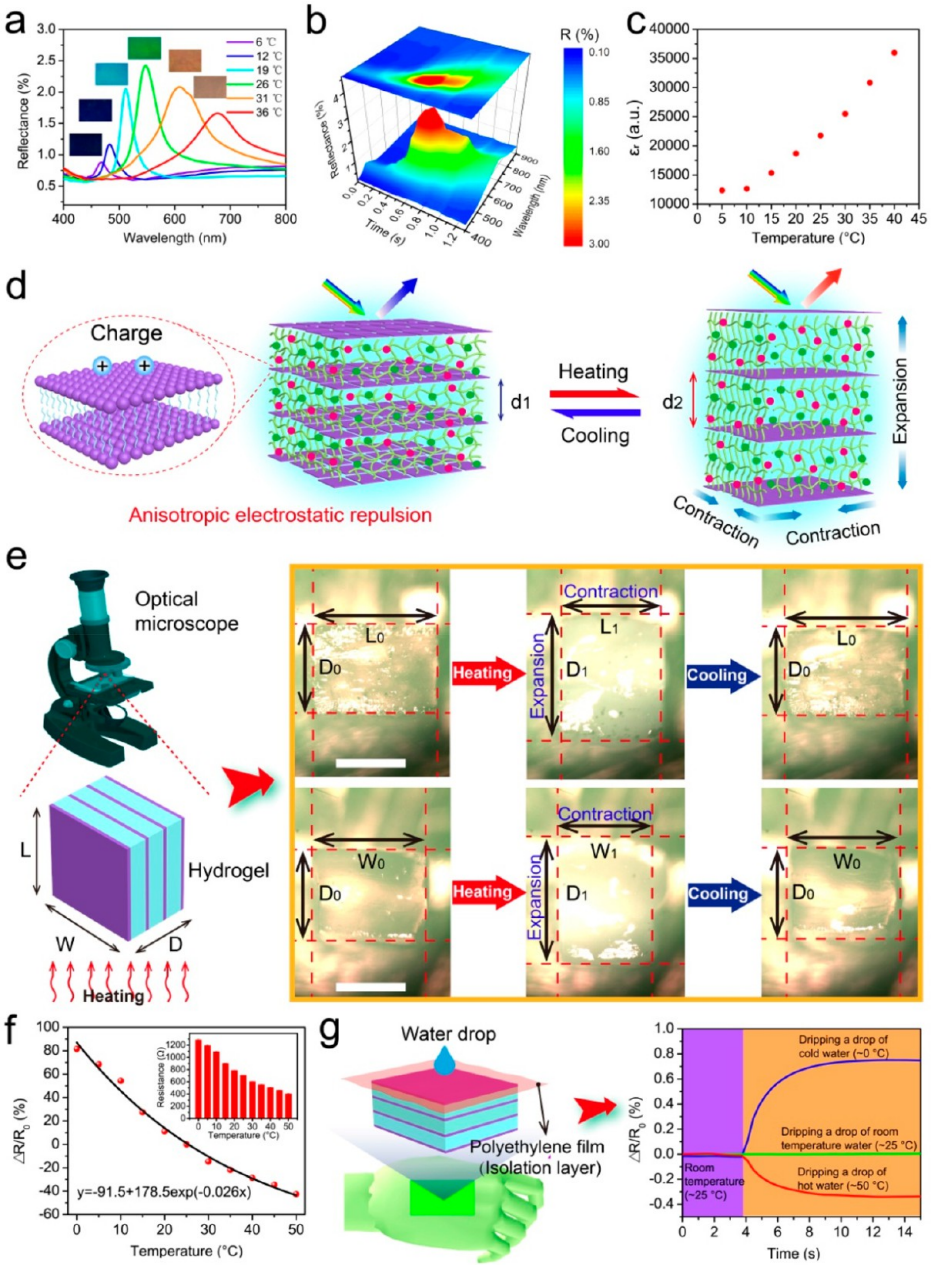

Figure 4. Thermal response mechanism and optical/electrical signal changes of ICPH. (a) Reflection spectra of the ICPH at different temperatures. Insets are the corresponding photographs of structural color. (b) Dynamic change of the reflection spectra with time from ~10 °C to ~40 °C. (c) Temperature-dependent change of the electrostatic permittivity of the PDAAM-*co*-PAAM hydrogel at a frequency of 10 kHz. (d) Mechanism illustration showing the anisotropic volume change and thermochromism regulated by electrostatic repulsion. (e) Schematic diagram and static microscope images of anisotropic volume change during the heating/cooling cycle (20−40 °C). Scale bar is 1 mm. (f) Relative resistance change of the ICPH at different temperatures. Inset is measured values of the resistance. R_0 is the resistance value at 25 °C. (g) Schematic diagram and relative resistance changes perceiving the temperature of a water drop (30 μL). During the test, a polyethylene film (thickness, 10 μm) was covered on the sample (22 mm × 12 mm × 2.1 mm) to prevent direct contact between the sample and the water drop. The ambient temperature is 25 °C.

convex seals, respectively (Figure 3i). This result indicates that the ICPH could visually identify the shape and location of the pressure source. Particularly, the gradient color change (letters "DUT") in response to the gradient strain demonstrated the ability to record a complex spatial distribution of pressure (Figure 3j).

Thermal Response Characteristics of ICPHs. ICPHs exhibit not only excellent mechanochromic properties but also sensitive and ultrafast temperature responsiveness. Traditional temperature-sensitive photonic hydrogels regulate color by swelling/deswelling of the hydrogel matrix, in which the response time is slow (several minutes to several hours) and increases with volume squared.[37−39,50,51] In sharp contrast, our ICPHs display ultrafast color-switching capability in response to temperature, which is critical for visually monitoring temperature in real time. For example, the reflection wavelength of the green sample (550 nm at 26 °C) blue-shifts to 467 nm at 6 °C, while gradually red-shifting to 677 nm at 36 °C (Figure 4a). The reflection wavelength varies continuously and rapidly from red to blue (Figure 4b and

https://dx.doi.org/10.1021/acsnano.1c00181
ACS Nano 2021, 15, 3509−3521

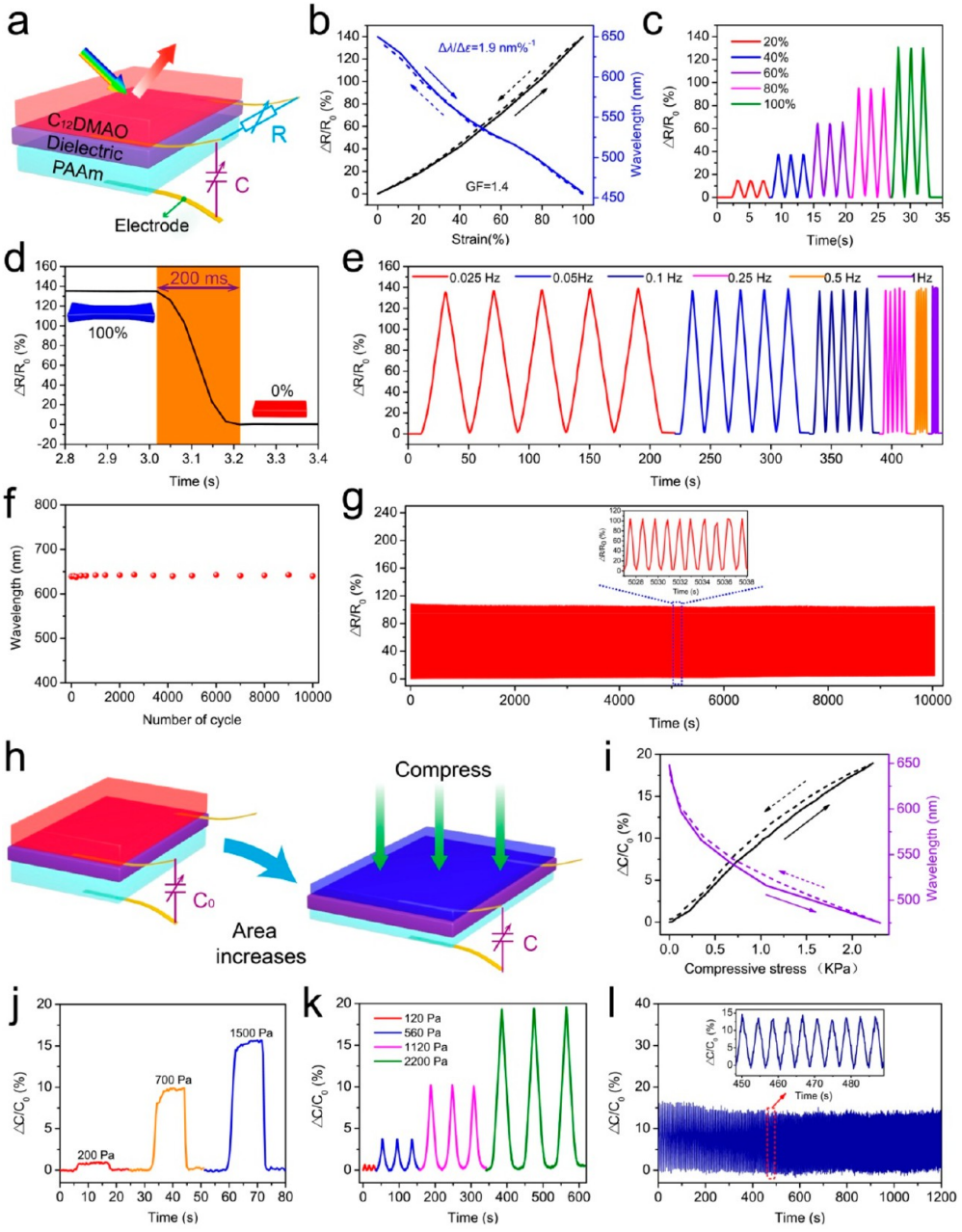

Figure 5. Sensing behavior of biomimetic CIskin to mechanical force. (a) Schematic diagram and two simplified equivalent circuits of the ionic sensory system. (b) Reversible changes in relative resistance and reflection wavelength with strain. (c) Relative resistance changes at different strains. (d) Self-recovery time of the relative resistance signal from 100% to 0%. Insets are schematic diagrams of the device under 100% and 0% strain, respectively. (e) Relative resistance changes with different tensile frequencies at 100% tensile strain. (f) Reflection wavelength of the device after different stretching/releasing cycles at 100% strain. (g) Change of relative resistance during 10 000 stretching/releasing cycles at a frequency of ∼1 Hz and a strain of 75%. (h) Mechanism illustration of capacitance change. (i) Reversible changes in relative capacitance and reflection wavelength with compressive stress. (j) Relative capacitance curve under stepwise compressive stress. (k) Relative capacitance changes at different compressive stress. (l) Change of relative capacitance during 300 cycling tests at a frequency of ∼0.25 Hz and a pressure of 1.7 kPa.

Figure S8). In particular, Movie S2 indicates that the ICPH exhibits a response time as short as ∼0.1 s from blue to red under a large temperature difference, much faster than conventional counterparts based on a swelling/deswelling mechanism *via* mass diffusion. This ultrafast thermal response speed endows the ICPH with visual real-time temperature monitoring, timely warning, and avoiding damage from high or low temperatures. We attribute this ultrafast response to the anisotropic electrostatic repulsion mechanism between positively charged bilayers. The potential energy (P) of an electrostatic repulsive force between bilayers is given by the following relationship:

$$P \propto \exp\left(-\frac{Cd}{\sqrt{\varepsilon_r T}}\right) \tag{2}$$

in which C is a constant, d represents the lattice spacing, ε_r denotes the electrostatic permittivity of the hydrogel matrix,

https://dx.doi.org/10.1021/acsnano.1c00181
ACS Nano 2021, 15, 3509−3521

and T is the temperature.[52] As shown in Figure 4c,d, the electrostatic permittivity ε_r of the hydrogel matrix (PDAAM-*co*-PAAM) increases with rising temperature T, leading to the enhancement of electrostatic repulsion between bilayers,[52,53] thus enlarging their spacing. This microscopic electrostatic repulsion caused a macroscopic increase of hydrogel thickness D (perpendicular to bilayers) and a decrease of length L and width W. As a result, the structural color has a red-shift. The phenomenon can also be confirmed by the shift of the scattering peak to the low-q regime in the SAXS profile, which indicates the increased bilayer spacing (Figure S9). Besides, such anisotropic deformation is reversible without external water uptake and release during heating/cooling, as demonstrated by optical microscope observation (Figure 4e, Movies S3 and S4, and Figure S10). In contrast, the pure PDAAM-*co*-PAAM matrix does not exhibit uniaxial expansion or contraction under the temperature change (Figure S11 and Movie S5), further supporting the above anisotropic electrostatic repulsion mechanism. We believe this mechanism provides an innovative route for the development of fast temperature responsive PCs.

The resistance of the ICPH decreases accompanying the red-shift of structural color with increasing the temperature, due to the increase of ionic mobility and the anisotropic deformation. Resistance can be expressed by the following equation:

$$R = C \exp\left(\frac{Q}{KT}\right)\frac{L}{A} \tag{3}$$

in which C, Q, K, L, and A denote the fitting constant, the activation energy, the Boltzmann constant, the length of the hydrogel, and the cross-sectional area of the hydrogel,[54] respectively. Assuming that the volume of the ICPH remains constant at different temperatures (that is, volume = LA = L_0A_0), the formula of relative resistance variation can be derived from eq 3:

$$\frac{\Delta R}{R_0} = \exp\left(\frac{Q}{KT} - \frac{Q}{KT_0}\right)\left(\frac{L}{L_0}\right)^2 - 1 \tag{4}$$

where R_0 is defined as the resistance at 298 K, T is the test temperature, T_0 is 298 K, L is the test length of the ionic conductor, and L_0 is the length of the ionic conductor at 298 K. It can be seen from the formula that the relative resistance is related to temperature T and length L. With increasing T, the anisotropic deformation occurs to the ICPH, resulting in the decrease of L and thus the decrease of relative resistance. Therefore, the temperature and the anisotropic deformation together contribute to the reduction in resistance. Figure 4f shows the change of relative resistance in the temperature range of 0−50 °C. It is observed that the relative resistance decreased exponentially with increasing temperature, implying its high temperature sensitivity.[55] This temperature sensitivity even enables ICPH to respond to a water drop of different temperatures. As shown in Figure 4g, different temperatures of a droplet (0, 25, and 50 °C) produced corresponding relative resistance changes, when the ICPH was originally at room temperature (25 °C). Interestingly, the hydrogel can even provide a noncontact electrical response to heat exhaled from a human (*e.g.*, mouth breathing, Figure S12).

Biomimetic Multifunctional and Self-Displaying Ionic Sensory System. To obtain multifunctional biomimetic CIskin, we constructed an ionic sensory system by sandwiching a dielectric elastomer (Ecoflex00-30 doped with a small amount of carbon black) between the ICPH and PAAM hydrogel (Figure 5a and Figure S13).[8,34] The ionic resistance and capacitance can be obtained by connecting different electrodes as shown in Figure 5a. Meanwhile, ICPH provides optical signals and endows the system with a color-switching capability, and the black dielectric elastomer prevents the background color from interfering with structural color. The ionic sensory system can respond to stretching through optical and relative resistance dual signals. As shown in Figure 5b, optical and relative resistance signals change linearly with tensile strain and exhibit good reversibility. The mechanochromic sensitivity is ∼1.9 nm%$^{-1}$ and the gauge factor (GF) is ∼1.4, indicating that users can perceive external tensile strain *via* color and ionic signal changes simultaneously. Stable and repeatable relative resistance signals of the ionic sensory system under different strains reveal that the system can recognize mechanical deformation of different amplitudes (Figure 5c). In addition, the system has a fast response time of ∼200 ms (Figure 5d and Figure S14) under self-recovery conditions, ensuring that the user can monitor deformation movements in real time by the instrument and the naked eye. Low-frequency dependence is also exhibited because of its excellent elasticity (Figure 5e), implying stable output of the signal under complex movement. In particular, there is almost no drift in the reflection wavelength and relative resistance change during 10 000 stretching/releasing cycles (Figure 5f,g), showing excellent durability, repeatability, and long service life, which are necessary for practical applications.

At the same time, the ionic sensory system displays tactile-sensing capability through optical and relative capacitance signals (Figure 5h). The capacitance (C) can be given by the following equation:

$$C = \varepsilon_0\varepsilon_r\frac{S}{d} \tag{5}$$

in which ε_0 represents the vacuum dielectric constant, ε_r denotes the relative permittivity of the dielectric elastomer, S is the overlap area of two ionic hydrogels, and d is the thickness of the dielectric elastomer.[35] The capacitance of the ionic sensory system varies due to the changes of area S during compression (Figure S15), ignoring the change of d because the compression modulus of the elastomer is much higher than that of the hydrogel (Figure S16).[34,35] With increasing pressure, the hydrogels are continuously compressed and the area S increases gradually, so the relative capacitance ($\Delta C/C_0$ = $(C-C_0)/C_0$, where C is the test capacitance and C_0 is the initial capacitance) enhances, while structural color blue-shifts due to the decrease of lattice spacing, and the system recovers its original state after removing the pressure (Figure 5i). The changes of relative capacitance signals are stable and reproducible for different pressures (Figure 5j,k). The relative capacitance variation is almost consistent without obvious degradation during 300 continuous cycling tests at ∼1.7 kPa and a frequency of ∼0.25 Hz (Figure 5l), indicating the good reliability of this biomimetic skin in tactile sensing. In addition, two layers of VHB (4905, 3M) were attached to the top and bottom of the sensor to limit the volatilization of water in the hydrogels (Figure S17).[6,8,34]

Applications as a Multifunctional Biomimetic Skin with Interactive Ability. As a proof-of-concept experiment, we demonstrate the application of an ionic sensory system as a cephalopod-like biomimetic skin in a personalized prosthesis,

https://dx.doi.org/10.1021/acsnano.1c00181
ACS Nano 2021, 15, 3509−3521

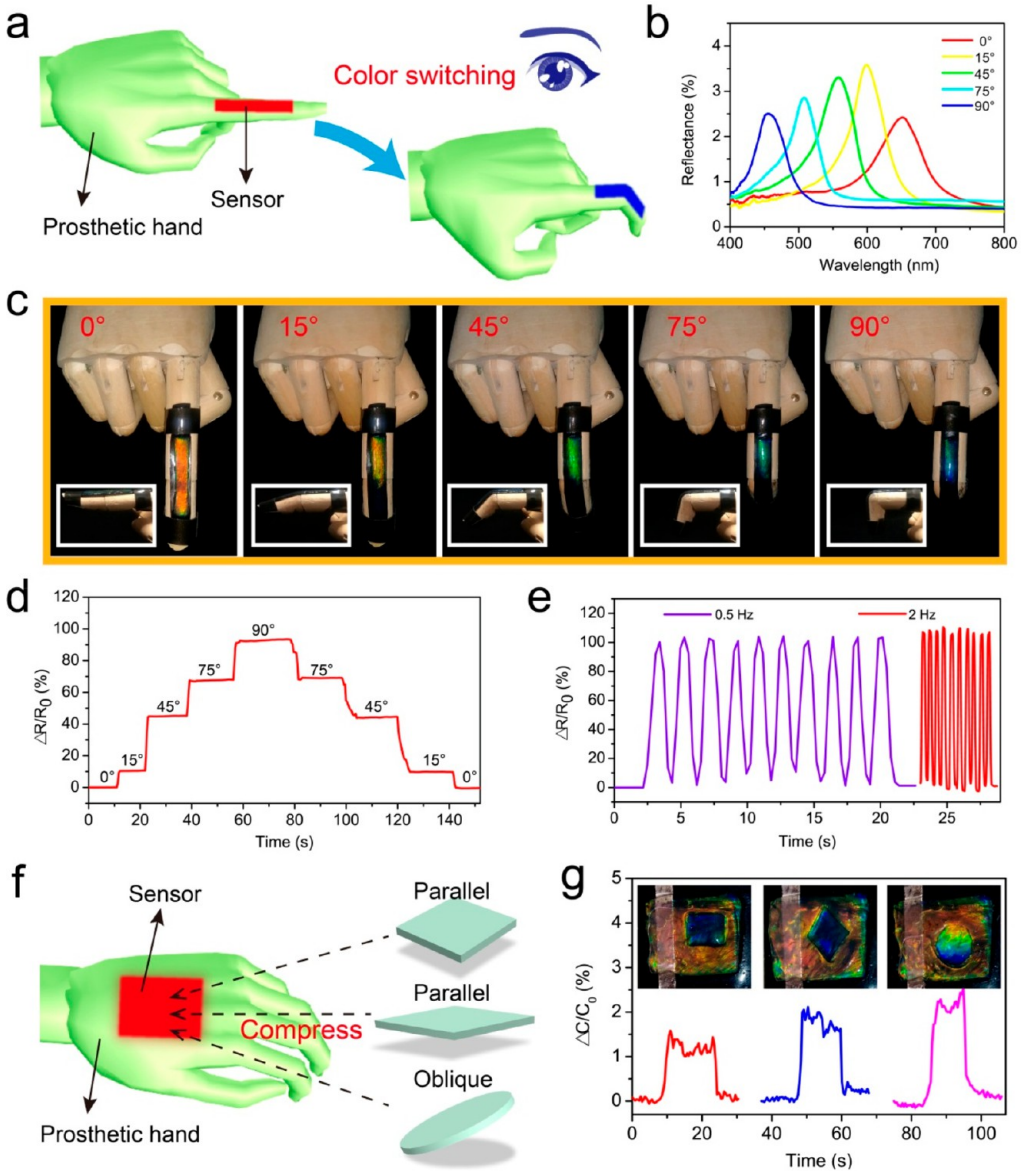

Figure 6. Applications of the biomimetic CIskin in strain and tactile sensation. (a) Schematic diagram monitoring joint movement of the index finger. (b–d) Reflection spectra (b), photographs (c), and the corresponding relative resistance (d) of the biomimetic skin attached to a finger under stepwise bending. Insets reflect side-views of the finger. (e) Real-time relative resistance changes sensing finger bending behavior at low (0.5 Hz) and high (2 Hz) frequencies. (f, g) Schematic diagram showing tactile sensation (f) and relative capacitance responses (g) to different pressure sources. Insets show the corresponding structural color changes.

which can sense external stimuli such as strain, tactile sensation, temperature, and IR light. As shown in Figure 6a, the device is attached to index finger of a prosthetic hand to monitor bending movement. As the finger stepwise bends, the reflection wavelength decreases and the structural color blue-shifts (Figure 6b,c and Movie S6). Synchronously, the relative resistance signal presents a stepwise upgrade, indicating that the biomimetic skin can precisely recognize the bending of the finger (Figure 6d). In addition, the device provides repeatable and stable relative resistance signal changes, regardless of the bending frequency (Figure 6e). The above results prove that the biomimetic skin can not only accurately record and recognize the motion state through electrical signals but also continuously and quantitatively visualize the motion information *via* colors. Analogous electrical and optical signals can also be obtained when the device is attached to a human index finger (Figure S18 and Movie S7). Furthermore, the device is attached to the back of a prosthetic hand to act as artificial skin. It can not only sense the external pressure but also identify the shape, position, and spatial distribution of the pressure source by displaying optical information. As shown in Figure 6f and g, when the pressure sources with different shapes (square, diamond, and ellipse) are applied, the capacitance response is presented in real time. The shape, location, and stress distribution can be shown by regional color changes (*e.g.*, square, diamond) and gradient distribution (*e.g.*, ellipse). Compared with conventional complex flexible sensors based on arrays, such an ability greatly simplifies the construction of the device and imparts a visual information display, thus realizing direct interaction with the user.

With the virtue of the ultrafast thermal response characteristic of ICPH, the biomimetic CIskin can further be used for

https://dx.doi.org/10.1021/acsnano.1c00181
ACS Nano 2021, 15, 3509–3521

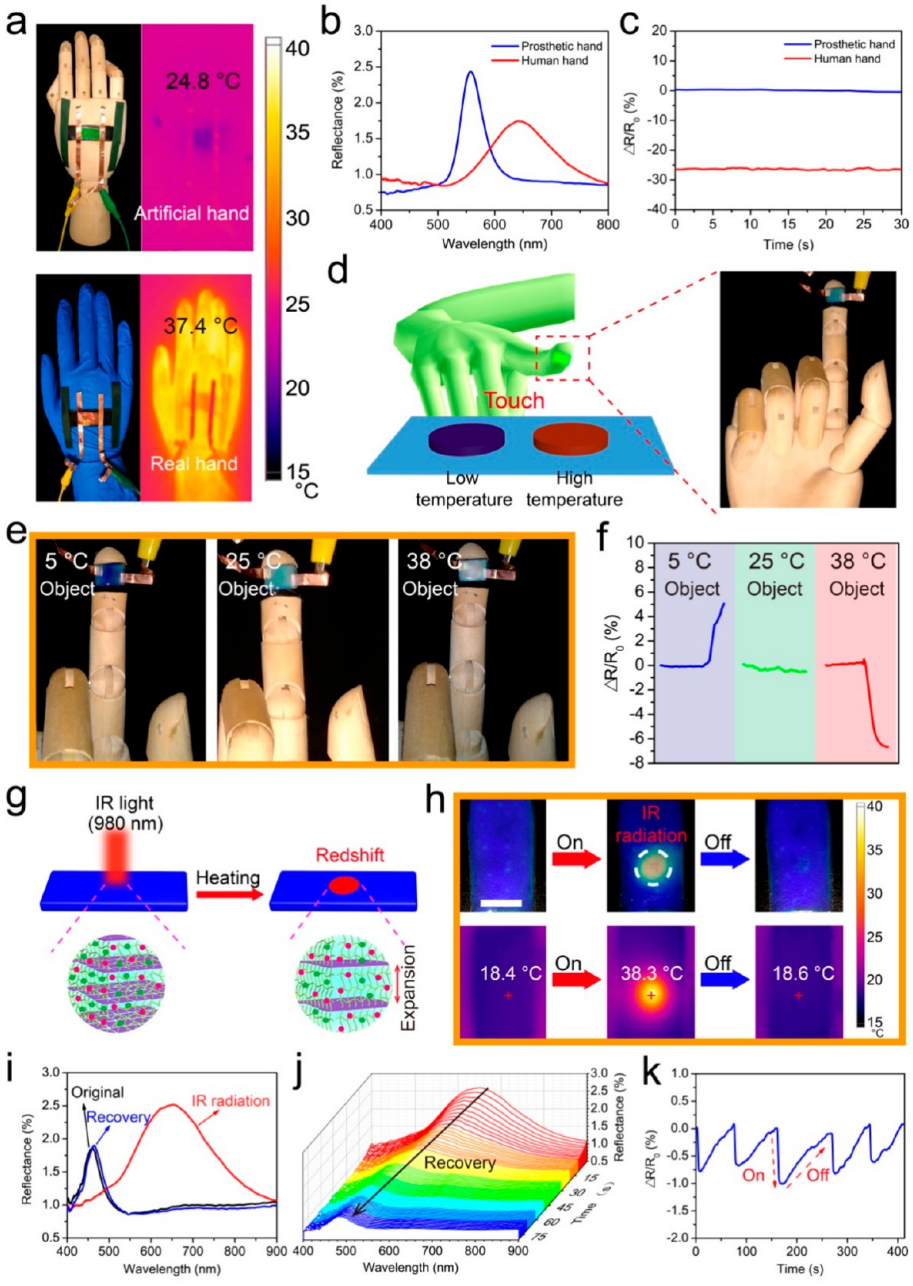

Figure 7. Applications of the biomimetic CIskin in temperature and IR light sensing. (a–c) Photographs and infrared images (a), reflection spectra (b), and relative resistances (c) of the biomimetic skin pasted on a prosthetic and human hand, respectively. R_0 is the resistance value at 25 °C. (d) Schematic diagram showing the device as a sensor cell touching objects with different temperatures. (e, f) Structural color changes (e) and relative resistance responses (f) of the sample after touching objects with different temperatures. (g) Mechanism illustration showing IR light response. (h) Structural color and temperature changes of the biomimetic skin irradiated by IR light (0.3 w/mm^2) for 2 s. Top is the photographs of the sample before and after IR irradiation, and bottom is the corresponding infrared images. Scale bar is 1 cm. (i) Reflection spectra of the sample before and after IR irradiation in (h). (j) Continuous change in the reflection spectra during recovery after IR light removal. (k) Relative resistance response periodically irradiated by IR light.

interactive temperature sensing. Here, we use the green ICPH (25 °C) to construct an ionic sensory system to perceive temperature to achieve the thermochromic function from red to blue. As shown in Figure 7a–c, our device exhibits the differences of relative resistance and optical signals on a prosthetic and human hand, respectively, because of the different body temperature. Moreover, the biomimetic skin can quickly sense the temperature of a contacted object and timely provide feedback to users, which is conducive to avoiding the harm of uncomfortable temperature to the human or prosthesis. For instance, the device is used as a sensory cell of the prosthesis to touch objects with different temperatures (Figure 7d). When it is gently in contact with low-temperature (5 °C) and high-temperature (38 °C) objects, the structural color switches to blue and red, respectively (Figure 7e). On the contrary, there is no change when it encounters an object at the same temperature (25 °C). At the same time, the relative resistance changes in a corresponding trend in response to the temperature change (Figure 7f). Furthermore, the biomimetic skin displays optical and electrical responses to IR light

https://dx.doi.org/10.1021/acsnano.1c00181
ACS Nano 2021, 15, 3509–3521

through the photothermal effect. As demonstrated in Figure 7g and Movie S8, the skin is heated when exposed to a 980 nm IR light, resulting in an increase in the bilayer spacing and a red-shift of the structural color. For example, we used IR light to irradiate a sample for 2 s, the temperature of the irradiation area increased rapidly from 18 to 38 °C, along with the red-shift of the structural color from 460 to 650 nm (Figure 7h,i). After irradiation removal, its structural color returns to the original state *via* heat dissipation (Figure 7j). Expectedly, the relative resistance of the sample irradiated by IR light will also decrease due to temperature rise. As shown in Figure 7k, the electrical output signal changes periodically with the periodic irradiation. Our CIskin can differentiate different stimuli by comparing the changes in color and capacitance. It can be seen from Figure S19 that when the device is subjected to different external stimuli, its color can be switched from red to blue. However, the capacitance change caused by a stretching stimulus is ∼100%, and that caused by compression is only ∼19%, while the temperature hardly leads to a capacitance change (see the detailed description in the Supporting Information). In addition, our device acts as an interactive CIskin, the change and spatial distribution of structural color can provide the basis for stimulus recognition.[33] For example, when the finger is bent, the tensile strain at the joint is the largest and the overall color presents a gradient change at the joint (Figure 6c, Figure S18b, Movies S6 and S7). When the color of a certain area is blue-shifted and the surrounding area does not change, the stimulus is pressure (Figure 6g). When the ambient temperature is changed, the color of CIskin shows an overall change (Figure 7a). On the other hand, the color of a certain area has a radioactive red-shift due to the conduction of heat to the surrounding area, which indicates that the stimulus is IR light (Figure 7h). The above discussion indicates that our biomimetic CIskin provides a self-displaying platform that could report diverse external stimuli and achieve visual interaction with users in real time.

CONCLUSION

In conclusion, by fully mimicking cephalopod skin, we have successfully demonstrated a CIskin with quadruple sensory abilities (strain, tactile sensation, temperature, and IR light) based on a multifunctional ionic-conductive photonic hydrogel with anisotropic electrostatic repulsion. The ICPH is developed by embedding artificial reflective plates (charged C_{12}DMAO 2D bilayers) in a permittivity-switchable PDAAM-*co*-PAAM matrix, which provides bright structural colors derived from Bragg diffraction. The biomimetic skin is capable of producing rapid, reversible resistance signal variation and continuous color switching from red to blue under tensile strain, which accurately records the joint movements of a prosthesis and the human body, and achieve visual quantification by real-time color transduction. Furthermore, our CIskin displays dual-signal reporting characteristics for tactile sensation, achieving a self-displaying spatial distribution of the pressure. More importantly, our biomimetic skin possesses an ultrafast optical response to thermal stimuli (∼0.1 s) through the anisotropic electrostatic repulsion mechanism between positively charged bilayers, enabling timely visual capture of temperature and IR light. We believe that this work provides general inspiration for visualization and smart interaction of soft iontronics to multiple stimuli, which would expand its application with higher-level functionality in smart prosthetics, wearable flexible devices, soft intelligent robots, human−machine interfaces, and other fields.

METHODS

Materials. A C_{12}DMAO (30 wt %) solution in H_2O was purchased from J&K Chemicals. AAM, DAAM, *n*-hexanol, MBAA, photoinitiator diphenyl (2,4,6-trimethylbenzoyl)phosphine oxide (TPO), and 2-hydroxy-2-methylpropiophenone (1173) were purchased from Aladdin Chemical Co. Ecoflex 00-30 was purchased from Smooth-On, Inc.

Preparation of Ionic-Conductive Photonic Hydrogels. First, C_{12}DMAO (60 mg), *n*-hexanol (85 mg), DAAM (0.5 g), AAM (0.25 g), MBAA (2−12 mg), and TPO (2.5 mg) were added into deionized water (5 mL). After ultrasonic treatment (20 min), the precursors were kept at ∼15 °C. Second, 1 mm thick double-adhesive tape was sandwiched between two glass plates to form a reaction cell. Subsequently, the precursor was injected into the reaction cell and then photocured with a 365 nm UV lamp (12 W) at 15 °C for 5 min. Then, the obtained hydrogel was immersed in deionized water for 3 days to achieve swelling equilibrium and unreacted chemicals were washed away, showing a bright structural color. Finally, the ICPH was obtained by soaking the above hydrogel in a NaCl aqueous solution (1, 2, 3, and 4 wt %) for 24 h to introduce conductive ions. NaCl content in ICPH can be measured by ion chromatography (Figure S20).

Preparation of the PAAM Ionic Hydrogel. First, AAM (720 mg), MBAA (2 mg), and photoinitiator 1173 (2.5 mg) were dissolved in deionized water (5 mL). Then, the precursor was injected into the sandwiched reaction cell (thickness, 0.5 mm), followed by UV photocuring for 5 min. Ultimately, the PAAM ionic hydrogel was obtained by immersing in a 2 wt % NaCl solution for 24 h.

Construction of the Biomimetic Ionic Sensory System. First, parts A and B of Ecoflex 00-30 were mixed at a mass ratio of 1:1; then 0.5 wt % carbon black was added and stirred for 10 min. The obtained precursor was poured into a concave groove with a wall height of 0.5 mm. The dielectric elastomer was obtained after curing for 4 h at room temperature. Second, ethyl cyanoacrylate adhesive was dispersed in cyclohexane (mass ratio 1:5) as an adhesive dispersion,[56] which was applied on the dielectric elastomer surface. Finally, the biomimetic skin was obtained by gluing the ICPH and PAAM hydrogels onto both sides of the elastomer, respectively. In order to ensure the effectiveness of the biomimetic skin during compression, the area of the elastomer was much larger than that of the ICPH and PAAM hydrogels.

Characterization and Measurements. The TEM image was taken by a HT7700 EXALENS. The SAXS measurement of the ICPH was carried out using a NanoSTAR instrument at the Testing Center of Yangzhou University. The normal-incidence reflection spectrum and the changes in light reflection intensity at a specified wavelength were obtained using a PG2000-Pro fiber-optic spectrometer (Shanghai Ideaoptics Corp., Ltd.). All digital images are taken vertically. The mechanical tensile/compression tests were carried out by a universal testing machine (PT-305, Dongguan Precise-Test Equipment Co., Ltd.). Tensile and compression rates were 20 and 1 mm/min, respectively. Compressive stress is defined as the applied force divided by the area of the undeformed ICPH. The repeat stretching/releasing test was performed by a homemade cyclic tensile tester with adjustable frequency. Two layers of VHB (thickness, 0.5 mm) were attached to the top and bottom of the sensor to prevent water evaporation during the test.[8] Resistance and capacitance measurements were performed using an LCR meter (TH2833) with a voltage of 1 V and a sweep frequency of 1 kHz. Movies and static images of the anisotropic volume changes of hydrogels were photographed by a metallographic microscope (MIT300/500, Cnoptec). Infrared images were taken by a thermal infrared imager (TiS75, FLUKE). Zeta potential was measured by a Zeta potential analyzer (ZS90).

https://dx.doi.org/10.1021/acsnano.1c00181
ACS Nano 2021, 15, 3509−3521

ASSOCIATED CONTENT

Supporting Information

The Supporting Information is available free of charge at https://pubs.acs.org/doi/10.1021/acsnano.1c00181.

Properties of solution; components of solutions; SAXS profile; image of unswollen hydrogel; distance between the bilayers; influence of NaCl solutions on color; mechanism illustration; changes of the reflection spectrum; SAXS profiles at different temperatures; weight change; change in the volume; response to heat exhaled; integration of the device; response time; area change; compression stress−strain curves; stability tests; responses to a human finger; dual-signal changes; NaCl content (PDF)

Movie S1: dynamic color change during compression (MP4)

Movie S2: color change from blue to red within ∼0.1 s at a large temperature difference (MP4)

Movie S3: reversible anisotropic deformation of length and thickness of the ICPH (MP4)

Movie S4: reversible anisotropic deformation of width and thickness of the ICPH (MP4)

Movie S5: change in the volume of the pure PDAAM-*co*-PAAM matrix (MP4)

Movie S6: dynamic color change during finger bending of the prosthesis (MP4)

Movie S7: dynamic color switching during finger bending of the human. (MP4)

Movie S8: a visual response to IR light (MP4)

AUTHOR INFORMATION

Corresponding Authors

Wenbin Niu − *State Key Laboratory of Fine Chemicals, Dalian University of Technology, Dalian 116024, China;* orcid.org/0000-0001-5507-1592; Email: niuwb@dlut.edu.cn

Ximin He − *Department of Materials Science and Engineering, University of California, Los Angeles, California 90095, United States;* orcid.org/0000-0001-8845-4637; Email: ximinhe@ucla.edu

Authors

Yunpeng Wang − *State Key Laboratory of Fine Chemicals, Dalian University of Technology, Dalian 116024, China*

Xianfei Cao − *State Key Laboratory of Fine Chemicals, Dalian University of Technology, Dalian 116024, China*

Jie Cheng − *State Key Laboratory of Fine Chemicals, Dalian University of Technology, Dalian 116024, China*

Bowen Yao − *Department of Materials Science and Engineering, University of California, Los Angeles, California 90095, United States*

Yusen Zhao − *Department of Materials Science and Engineering, University of California, Los Angeles, California 90095, United States*

Suli Wu − *State Key Laboratory of Fine Chemicals, Dalian University of Technology, Dalian 116024, China;* orcid.org/0000-0002-3956-1855

Benzhi Ju − *State Key Laboratory of Fine Chemicals, Dalian University of Technology, Dalian 116024, China*

Shufen Zhang − *State Key Laboratory of Fine Chemicals, Dalian University of Technology, Dalian 116024, China;* orcid.org/0000-0003-3390-4199

Complete contact information is available at: https://pubs.acs.org/10.1021/acsnano.1c00181

Author Contributions

Y.W., S.W., B.J., S.Z., X.H., and W.N. conceived the project. Y.W. performed the experiments. Y.W. and W.N. wrote the paper with contributions of all authors. X.C. and J.C. participated in the performance testing of the device in the application section. Y.Z., B.Y., and X.H. analyzed and discussed the experimental data and results and commented on the manuscript.

Notes

The authors declare no competing financial interest.

ACKNOWLEDGMENTS

The work was financially supported by National Natural Science Foundation of China (22078048), Dalian High-level Talents Innovation Support Program (2019RD06, 2019RQ142), the Liaoning Revitalization Talent Program (1801006), and the Fundamental Research Funds for the Central Universities (DUT19JC14, DUT2019TA06).

REFERENCES

(1) Ranade, S. S.; Syeda, R.; Patapoutian, A. Mechanically Activated Ion Channels. *Neuron* **2015**, *87*, 1162−1179.

(2) Jenkins, B. A.; Lumpkin, E. A. Developing a Sense of Touch. *Development* **2017**, *144*, 4078−4090.

(3) Toyota, M.; Spencer, D.; Sawai-Toyota, S.; Wang, J. Q.; Zhang, T.; Koo, A. J.; Howe, G. A.; Gilroy, S. Glutamate Triggers Long-Distance, Calcium-Based Plant Defense Signaling. *Science* **2018**, *361*, 1112−1115.

(4) Jin, M. L.; Park, S.; Lee, Y.; Lee, J. H.; Chung, J.; Kim, J. S.; Kim, J. S.; Kim, S. Y.; Jee, E.; Kim, D. W.; Chung, J. W.; Lee, S. G.; Choi, D.; Jung, H. T.; Kim, D. H. An Ultrasensitive, Visco-Poroelastic Artificial Mechanotransducer Skin Inspired by Piezo2 Protein in Mammalian Merkel Cells. *Adv. Mater.* **2017**, *29*, 1605973.

(5) Xiao, K.; Wan, C.; Jiang, L.; Chen, X.; Antonietti, M. Bioinspired Ionic Sensory Systems: The Successor of Electronics. *Adv. Mater.* **2020**, *32*, 2000218.

(6) Ying, B.; Wu, Q.; Li, J.; Liu, X. An Ambient-Stable and Stretchable Ionic Skin with Multimodal Sensation. *Mater. Horiz.* **2020**, *7*, 477−488.

(7) Zhang, X.; Sheng, N.; Wang, L.; Tan, Y.; Liu, C.; Xia, Y.; Nie, Z.; Sui, K. Supramolecular Nanofibrillar Hydrogels as Highly Stretchable, Elastic and Sensitive Ionic Sensors. *Mater. Horiz.* **2019**, *6*, 326−333.

(8) Sun, J. Y.; Keplinger, C.; Whitesides, G. M.; Suo, Z. Ionic Skin. *Adv. Mater.* **2014**, *26*, 7608−7614.

(9) Lee, H.-R.; Kim, C.-C.; Sun, J.-Y. Stretchable Ionics - A Promising Candidate for Upcoming Wearable Devices. *Adv. Mater.* **2018**, *30*, 1704403.

(10) Yang, C.; Suo, Z. Hydrogel Ionotronics. *Nat. Rev. Mater.* **2018**, *3*, 125−142.

(11) Yoshioka, S.; Matsuhana, B.; Tanaka, S.; Inouye, Y.; Oshima, N.; Kinoshita, S. Mechanism of Variable Structural Colour in the Neon Tetra: Quantitative Evaluation of the Venetian Blind Model. *J. R. Soc., Interface* **2011**, *8*, 56−66.

(12) Mäthger, L. M.; Senft, S. L.; Gao, M.; Karaveli, S.; Bell, G. R. R.; Zia, R.; Kuzirian, A. M.; Dennis, P. B.; Crookes, G. W. J.; Naik, R. R.; Kattawar, G. W.; Hanlon, R. T. Bright White Scattering from Protein Spheres in Color Changing, Flexible Cuttlefish Skin. *Adv. Funct. Mater.* **2013**, *23*, 3980−3989.

(13) Hanlon, R. T.; Chiao, C. C.; Mäthger, L. M.; Barbosa, A.; Buresch, K. C.; Chubb, C. Cephalopod Dynamic Camouflage: Bridging the Continuum between Background Matching and Disruptive Coloration. *Philos. Trans. R. Soc., B* **2009**, *364*, 429−437.

(14) Teyssier, J.; Saenko, S. V.; van der Marel, D.; Milinkovitch, M. C. Photonic Crystals Cause Active Colour Change in Chameleons. *Nat. Commun.* **2015**, *6*, 6368.
(15) Lee, G. H.; Choi, T. M.; Kim, B.; Han, S. H.; Lee, J. M.; Kim, S.-H. Chameleon-Inspired Mechanochromic Photonic Films Composed of Non-Close-Packed Colloidal Arrays. *ACS Nano* **2017**, *11*, 11350−11357.
(16) Stuart, F. D.; Moussalli, A. Camouflage, Communication and Thermoregulation: Lessons from Colour Changing Organisms. *Philos. Trans. R. Soc., B* **2009**, *364*, 463−470.
(17) Stuart, F. D.; Moussalli, A. Selection for Social Signalling Drives the Evolution of Chameleon Colour Change. *PLoS Biol.* **2008**, *6*, 22−29.
(18) Zhao, Y.; Xie, Z.; Gu, H.; Zhu, C.; Gu, Z. Bio-Inspired Variable Structural Color Materials. *Chem. Soc. Rev.* **2012**, *41*, 3297−3317.
(19) Fenzl, C.; Hirsch, T.; Wolfbeis, O. S. Photonic Crystals for Chemical Sensing and Biosensing. *Angew. Chem., Int. Ed.* **2014**, *53*, 3318−3335.
(20) Dumanli, A. G.; Savin, T. Recent Advances in the Biomimicry of Structural Colours. *Chem. Soc. Rev.* **2016**, *45*, 6698−6724.
(21) Chen, Z.; Fu, F.; Yu, Y.; Wang, H.; Shang, Y.; Zhao, Y. Cardiomyocytes-Actuated Morpho Butterfly Wings. *Adv. Mater.* **2019**, *31*, 1805431.
(22) Fu, F.; Shang, L.; Chen, Z.; Yu, Y.; Zhao, Y. Bioinspired Living Structural Color Hydrogels. *Sci. Robot.* **2018**, *3*, No. eaar8580.
(23) Hanlon, R. T.; Cooper, K. M.; Budelmann, B. U.; Pappas, T. C. Physiological Color Change in Squid Iridophores. I. Behavior, Morphology and Pharmacology in Lolliguncula Brevis. *Cell Tissue Res.* **1990**, *259*, 3−14.
(24) Kramer, R. M.; Crookes, G. W. J.; Naik, R. R. The Self-Organizing Properties of Squid Reflectin Protein. *Nat. Mater.* **2007**, *6*, 533−538.
(25) Zhang, L.; Liao, M.; Bao, L.; Sun, X.; Peng, H. The Functionalization of Miniature Energy-Storage Devices. *Small Methods* **2017**, *1*, 1700211.
(26) Chou, H. H.; Nguyen, A.; Chortos, A.; To, J. W. F.; Lu, C.; Mei, J. G.; Kurosawa, T.; Bae, W. G.; Tok, J. B. H.; Bao, Z. A. A Chameleon-Inspired Stretchable Electronic Skin with Interactive Colour Changing Controlled by Tactile Sensing. *Nat. Commun.* **2015**, *6*, 8011.
(27) Park, J.; Lee, Y.; Barbee, M. H.; Cho, S.; Cho, S.; Shanker, R.; Kim, J.; Myoung, J.; Kim, M. P.; Baig, C.; Craig, S. L.; Ko, H. A Hierarchical Nanoparticle-in-Micropore Architecture for Enhanced Mechanosensitivity and Stretchability in Mechanochromic Electronic Skins. *Adv. Mater.* **2019**, *31*, 1808148.
(28) Kim, G.; Cho, S.; Chang, K.; Kim, W. S.; Kang, H.; Ryu, S. P.; Myoung, J.; Park, J.; Park, C.; Shim, W. Spatially Pressure-Mapped Thermochromic Interactive Sensor. *Adv. Mater.* **2017**, *29*, 1606120.
(29) Yu, C.; Li, Y.; Zhang, X.; Huang, X.; Malyarchuk, V.; Wang, S.; Shi, Y.; Gao, L.; Su, Y.; Zhang, Y.; Xu, H.; Hanlon, R. T.; Huang, Y.; Rogers, J. A. Adaptive Optoelectronic Camouflage Systems with Designs Inspired by Cephalopod Skins. *Proc. Natl. Acad. Sci. U. S. A.* **2014**, *111*, 12998−13003.
(30) Zeng, S.; Sun, H.; Park, C.; Zhang, M.; Zhu, M.; Yan, M.; Chov, N.; Li, E.; Smith, A. T.; Xu, G.; Li, S.; Hou, Z.; Li, Y.; Wang, B.; Zhang, D.; Sun, L. Multi-Stimuli Responsive Chromism with Tailorable Mechanochromic Sensitivity for Versatile Interactive Sensing under Ambient Conditions. *Mater. Horiz.* **2020**, *7*, 164−172.
(31) Wang, Y.; Niu, W.; Lo, C. Y.; Zhao, Y.; He, X.; Zhang, G.; Wu, S.; Ju, B.; Zhang, S. Interactively Full-Color Changeable Electronic Fiber Sensor with High Stretchability and Rapid Response. *Adv. Funct. Mater.* **2020**, *30*, 2000356.
(32) Wang, Y.; Yu, Y.; Guo, J.; Zhang, Z.; Zhang, X.; Zhao, Y. Bio-Inspired Stretchable, Adhesive, and Conductive Structural Color Film for Visually Flexible Electronics. *Adv. Funct. Mater.* **2020**, *30*, 2000151.
(33) Zhang, Z.; Chen, Z.; Wang, Y.; Zhao, Y. Bioinspired Conductive Cellulose Liquid-Crystal Hydrogels as Multifunctional Electrical Skins. *Proc. Natl. Acad. Sci. U. S. A.* **2020**, *117*, 18310−18316.
(34) Lei, Z.; Wu, P. A Supramolecular Biomimetic Skin Combining a Wide Spectrum of Mechanical Properties and Multiple Sensory Capabilities. *Nat. Commun.* **2018**, *9*, 1134.
(35) Wang, C.; Xia, K.; Wang, H.; Liang, X.; Yin, Z.; Zhang, Y. Advanced Carbon for Flexible and Wearable Electronics. *Adv. Mater.* **2019**, *31*, 1801072.
(36) Chan, E. P.; Walish, J. J.; Urbas, A. M.; Thomas, E. L. Mechanochromic Photonic Gels. *Adv. Mater.* **2013**, *25*, 3934−3947.
(37) Hur, S.-T.; Lee, B. R.; Gim, M.-J.; Park, K.-W.; Song, M. H.; Choi, S.-W. Liquid-Crystalline Blue Phase Laser with Widely Tunable Wavelength. *Adv. Mater.* **2013**, *25*, 3002−3006.
(38) Yue, Y. F.; Haque, M. A.; Kurokawa, T.; Nakajima, T.; Gong, J. P. Lamellar Hydrogels with High Toughness and Ternary Tunable Photonic Stop-Band. *Adv. Mater.* **2013**, *25*, 3106−10.
(39) Chiappelli, M. C.; Hayward, R. C. Photonic Multilayer Sensors from Photo-Crosslinkable Polymer Films. *Adv. Mater.* **2012**, *24*, 6100−6104.
(40) Lim, H. S.; Lee, J. H.; Walish, J. J.; Thomas, E. L. Dynamic Swelling of Tunable Full-Color Block Copolymer Photonic Gels *via* Counterion Exchange. *ACS Nano* **2012**, *6*, 8933−8939.
(41) Haque, M. A.; Kamita, G.; Kurokawa, T.; Tsujii, K.; Gong, J. P. Unidirectional Alignment of Lamellar Bilayer in Hydrogel: One-Dimensional Swelling, Anisotropic Modulus, and Stress/Strain Tunable Structural Color. *Adv. Mater.* **2010**, *22*, 5110−5114.
(42) Platz, G.; Thunig, C.; Hoffmann, H. Iridescent Phases in Aminoxide Surfactant Solutions. *Prog. Colloid Polym. Sci.* **1990**, *83*, 167−175.
(43) Thunig, C.; Hoffmann, H.; Platz, G. Iridescent Colors in Surfactant Solutions. *Prog. Colloid Polym. Sci.* **1989**, *79*, 297−307.
(44) Hayakawa, M.; Onda, T.; Tanaka, T.; Tsujii, K. Hydrogels Containing Immobilized Bilayer Membranes. *Langmuir* **1997**, *13*, 3595−3597.
(45) Niu, J.; Wang, D.; Qin, H.; Xiong, X.; Tan, P.; Li, Y.; Liu, R.; Lu, X.; Wu, J.; Zhang, T.; Ni, W.; Jin, J. Novel Polymer-Free Iridescent Lamellar Hydrogel for Two-Dimensional Confined Growth of Ultrathin Gold Membranes. *Nat. Commun.* **2014**, *5*, 3313.
(46) Zeng, M.; King, D.; Huang, D.; Do, C.; Wang, L.; Chen, M.; Lei, S.; Lin, P.; Chen, Y.; Cheng, Z. Iridescence in Nematics: Photonic Liquid Crystals of Nanoplates in Absence of Long-Range Periodicity. *Proc. Natl. Acad. Sci. U. S. A.* **2019**, *116*, 18322−18327.
(47) Haque, M. A.; Kurokawa, T.; Kamita, G.; Gong, J. P. Lamellar Bilayers as Reversible Sacrificial Bonds to Toughen Hydrogel: Hysteresis, Self-Recovery, Fatigue Resistance, and Crack Blunting. *Macromolecules* **2011**, *44*, 8916−8924.
(48) Sun, J.-Y.; Zhao, X.; Illeperuma, W. R.; Chaudhuri, O.; Oh, K. H.; Mooney, D. J.; Vlassak, J. J.; Suo, Z. Highly Stretchable and Tough Hydrogels. *Nature* **2012**, *489*, 133−136.
(49) Qiao, H.; Qi, P.; Zhang, X.; Wang, L.; Tan, Y.; Luan, Z.; Xia, Y.; Li, Y.; Sui, K. Multiple Weak H-Bonds Lead to Highly Sensitive, Stretchable, Self-Adhesive, and Self-Healing Ionic Sensors. *ACS Appl. Mater. Interfaces* **2019**, *11*, 7755−7763.
(50) Eoh, H.; Kang, H. S.; Kim, M. J.; Koo, M.; Park, T. H.; Kim, Y.; Lim, H.; Ryu, D. Y.; Kim, E.; Huh, J.; Kang, Y.; Park, C. Nonvolatile, Multicolored Photothermal Writing of Block Copolymer Structural Color. *Adv. Funct. Mater.* **2019**, *29*, 1904055.
(51) Song, D.-P.; Li, C.; Colella, N. S.; Lu, X.; Lee, J.-H.; Watkins, J. J. Thermally Tunable Metallodielectric Photonic Crystals from the Self-Assembly of Brush Block Copolymers and Gold Nanoparticles. *Adv. Opt. Mater.* **2015**, *3*, 1169−1175.
(52) Kim, Y. S.; Liu, M.; Ishida, Y.; Ebina, Y.; Osada, M.; Sasaki, T.; Hikima, T.; Takata, M.; Aida, T. Thermoresponsive Actuation Enabled by Permittivity Switching in An Electrostatically Anisotropic Hydrogel. *Nat. Mater.* **2015**, *14*, 1002−1007.
(53) Sun, Z. F.; Yamauchi, Y.; Araoka, F.; Kim, Y. S.; Bergueiro, J.; Ishida, Y.; Ebina, Y.; Sasaki, T.; Hikima, T.; Aida, T. An Anisotropic Hydrogel Actuator Enabling Earthworm-Like Directed Peristaltic Crawling. *Angew. Chem., Int. Ed.* **2018**, *57*, 15772−15776.

https://dx.doi.org/10.1021/acsnano.1c00181
ACS Nano 2021, 15, 3509−3521

(54) Xu, S.; Vogt, D. M.; Hsu, W.-H.; Osborne, J.; Walsh, T.; Foster, J. R.; Sullivan, S. K.; Smith, V. C.; Rousing, A. W.; Goldfield, E. C.; Wood, R. J. Biocompatible Soft Fluidic Strain and Force Sensors for Wearable Devices. *Adv. Funct. Mater.* **2019**, *29*, 1807058.
(55) Kim, E. H.; Han, H.; Yu, S.; Park, C.; Kim, G.; Jeong, B.; Lee, S. W.; Kim, J. S.; Lee, S.; Kim, J.; Park, J. U.; Shim, W.; Park, C. Interactive Skin Display with Epidermal Stimuli Electrode. *Adv. Sci.* **2019**, *6*, 1802351.
(56) Wirthl, D.; Pichler, R.; Drack, M.; Kettlguber, G.; Moser, R.; Gerstmayr, R.; Hartmann, F.; Bradt, E.; Kaltseis, R.; Siket, C. M.; Schausberger, S. E.; Hild, S.; Bauer, S.; Kaltenbrunner, M. Instant Tough Bonding of Hydrogels for Soft Machines and Electronics. *Sci. Adv.* **2017**, *3*, No. e1700053.

https://dx.doi.org/10.1021/acsnano.1c00181
ACS Nano 2021, 15, 3509−3521